Journal of Cleaner Production 478 (2024) 143906

Contents lists available at ScienceDirect

Journal of Cleaner Production

journal homepage: www.elsevier.com/locate/jclepro

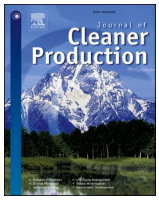

A cleaner demolition scheduling methodology considering dust dispersion: A case study for a post-earthquake region

Ali Ersin Dinçer [a], Abdullah Demir [b,*], Ömer Dilmen [a]

[a] Dep. of Civil Eng., Hydraulics Laboratory, Abdullah Gül University, Kayseri, 38080, Turkey
[b] Dep. of Civil Eng., Structural Laboratory, Abdullah Gül University, Kayseri, 38080, Turkey

ARTICLE INFO

Handling Editor: Jing Meng

Keywords:
Demolition
Dust dispersion
Dust exposure
Dust effect
AHP
MCDM

ABSTRACT

In the present century, pollution is a primary concern for billions, prompting governments to advocate cleaner ways of production. Demolition activity is often an indispensable solution for structures that have completed their economic life. However, there are no regulations for the scheduling of demolition, except those related to the method of demolition and ensuring worker safety. Older buildings incorporate hazardous materials, such as asbestos, silica, and lead. These materials not only carry inherent risks, but high levels of aerosols in the air also adversely affect health. In this study, a demolition scheduling method is proposed, considering the dust dispersion. This research is pioneering, providing a structured demolition schedule to minimize the impact on both humans and the environment. In the methodology, a dispersion model is used to calculate the region exposed to dust and the concentration distribution throughout that area. In addition to the dust effect map, a vulnerability map is created using Analytical Hierarchy Process (AHP), aiding in determining interrelations between vulnerable sites. Thus, the dust effect map is derived by considering both dust exposure and the vulnerability map. The region affected by dust and the concentration of dust vary based on wind characteristics. By knowing the dust effect maps for the site (or all subsites) during specified time periods, a schedule can be defined. As a case study, schedules causing the absolute minimum and optimum dust effect rates are established for Kahramanmaraş, Türkiye which recently experienced a devastating earthquake. The findings of the case study show that the dust effect on humans and the environment is significantly reduced. Consequently, by adhering to the proposed scheduling plan, human exposure to demolition dust is minimized, resulting in reduced medical expenses even without increasing the cost of the demolition.

1. Introduction

Demolition is the only solution for almost every damaged structure. Although there are some retrofitting techniques to restore functionality to a structure, the earthquake-induced damage is usually irreversible. The term “demolition” implies annihilating a structure. However, there is a lengthy recycling process before or after sweeping away the ruins from the structure’s site. If the structure has minimal damage, the term “deconstruction” can be used instead of “demolition” because the recycling process begins before destroying the structure, as a disassembling process. In contrast, it is not possible to initiate the recycling process before demolishing a severely damaged structure.

Although the main aim is to decrease the vulnerability of structures exposed to natural hazards (by minimizing the cost/benefit ratio), it is inevitable to have damaged structures after a hazardous earthquake. Depending on the location and soil conditions, the damaged structures can cluster or be individually scattered on the terrain. Therefore, the circumstances of the damaged structures decide the way of demolition. There are several ways for demolishing structures: by top down, wrecking ball, and implosion. Regardless of the way of demolition, dust is spread out by the wind, not only in the prevailing direction but also in the transverse direction. This will affect the region around the demolition site. The affected region mostly depends on the prevailing wind direction. Therefore, the season of demolition should be selected to minimize the dust exposure of citizens. Because, based on information given by doctors from Kahramanmaraş, where a devastating earthquake occurred on 6th February of 2023, hospital admissions for chest diseases increased by thirty percent.

In the literature, there is extensive research revealing the health effects of demolition. Apart from the increased dust concentrations in the

* Corresponding author. Dep. of Civil Eng., Structural Laboratory, Abdullah Gül University, Kayseri, 38080, Turkey
E-mail addresses: ersin.dincer@agu.edu.tr (A.E. Dinçer), abdullah.demir@agu.edu.tr (A. Demir), omer.dilmen@agu.edu.tr (Ö. Dilmen).

https://doi.org/10.1016/j.jclepro.2024.143906
Received 20 November 2023; Received in revised form 9 February 2024; Accepted 6 October 2024
Available online 9 October 2024
0959-6526/© 2024 Elsevier Ltd. All rights are reserved, including those for text and data mining, AI training, and similar technologies.

air, numerous harmful materials are dispersed around the city center. Some of these harmful materials are asbestos, silica, lead, and other heavy metals (Rodríguez et al., 2023). Demolition of buildings with asbestos containing materials (ACM) has been regulated since 1973 in the USA (Perkins et al., 2007). Although the use and marketing of ACM were prohibited in the EU in 1999 and in Türkiye in 2010 (Akboğa Kale et al., 2017), old buildings may still contain ACM, posing an inevitable risk of asbestos exposure.

In (Farfel et al., 2003; Mucha et al., 2009), lead contamination around demolition sites was examined, and (Rabito et al., 2007), reported a significant increase in children's blood lead levels. Similar to asbestos, silica in the form of crystalline silica dust poses risks of silicosis and an excess lifetime risk of mortality from lung cancer (Normohammadi et al., 2016). Additionally, lead and other heavy metals are also hazardous materials commonly used in construction in the past (Jacobs et al., 2013). Not only these specific harmful construction materials have negative health effects, but the dust dispersed around urban spaces also effects public health, causing issues like asthma (Dorevitch et al., 2006) and chronic lower respiratory diseases (Mølgaard et al., 2013).

In addition to these set-forth direct health effects (Rabito et al., 2007; Dorevitch et al., 2006; Mølgaard et al., 2013), demolition has indirect health effects due to dust effects in nature. Investigations were carried out to reveal the impact of dust in the air, water, and soil (Chu et al., 2011). A previous study disclosed the dust effect in an estuarine water in India caused by demolition (Menon et al., 2021). Despite existing studies on the hazardous health effects of demolition and investigations into the dispersion of hazardous materials, regulations for demolition are limited to considerations of workers' health (Patel and Patel, 2020) and solid waste disposal (Clark et al., 2006). There is a notable absence of regulations for demolition sites defining the season of demolition while considering the dispersion of dust with hazardous materials, causing health and environmental impacts.

Exposing particulate matter (PM), which is categorized into PM_{10}, $PM_{2.5}$ and PM_1 and based on size, have adverse impacts on human health as they may contain pollutants like heavy metals (Heal et al., 2012). To minimize exposure to particulate matter (PM), dust dispersion models should be employed to assess PM concentrations downstream from the demolition site. Various models have been proposed to simulate dust dispersion, ranging from simple box-type models to intricate fluid dynamics models (Holmes and Morawska, 2006). Dispersion modeling employs mathematical equations that depict atmospheric conditions, dispersion characteristics, and chemical and physical processes within the plume. Empirical and analytical solutions and numerical solutions of the advection-diffusion equations, random walk particle tracking models and buoyant jet type integral methods are used to model dispersion (Zhao et al., 2011). Analytical solutions, known as closed-form solutions, simplify derivations to solve governing equations (McCutcheon, 1990). Due to fluid hydrodynamics' complexity, assumptions are necessary, limiting their applicability to specific cases, such as regular, symmetrical geometry in flow solutions (Martin and McCutcheon, 1998). To overcome the limitations of analytical solutions, numerical solutions for advection diffusion equations can be preferred. Finite difference, finite volume and finite element methods are examples of numerical solutions. Rather than directly solving the advection–diffusion equation, the random walk particle tracking method addresses the transport equation by tracking individual particles as they traverse through space and time. In this method, advection is simulated by moving individual particles within the local fluid velocity field, and turbulent diffusion is replicated using a random walk technique (Periáñez and Elliott, 2002). The random walk particle tracking method handles the movement of solute mass through a multitude of particles, eliminating the need for numerical solution of the transport equation. Consequently, it minimizes numerical dispersion and artificial oscillations, resulting in fewer numerical errors and preserving the accuracy during particle tracking (Zhao et al., 2011; Salamon et al., 2006).

While researchers have concentrated on developing dispersion models to understand the impact of dust from building demolitions on human health and the environment, there is currently a lack of comprehensive studies proposing demolition plans that consider various criteria to minimize dust exposure. Although there are some governmental regulations for daily time periods for demolition activities, there is a lack of regulations defining the schedule for demolition activity.

In order to propose cleaner demolition regulations by defining schedules, a method for demolition scheduling is proposed, considering the health and environmental effects of dust dispersion. The study is pioneering research proposing a novel methodology to reveal the effects of demolition on nearby regions and scheduling the demolition activity that decreases the impact of dust dispersion. The algorithm involves using a dispersion model that integrates computational simulations with the Analytical Hierarchy Process (AHP) for multi-criteria decision-making, as well as GIS-based analysis, considering dynamic wind characteristics, to determine affected regions and optimize demolition time periods for subsites. Unit dust effects are calculated for inter-month and inter-subsite comparisons. Different scheduling scenarios are proposed, aiming to demolish each subsite in its optimum month or minimize the unit dust effect for efficient scheduling.

2. Methodology

In order to clearly state the main steps of the proposed methodology, the model used for dust dispersion and the Analytical Hierarchy Process (AHP) used to give multi-criteria decisions are defined in detail.

2.1. Dispersion model

In the present study, Sutherland-Einstein Diffusion Analysis (Sutherlan, 1904; Sutherland, 1905; Einstein, 1905) and a random walk particle tracking method (RWPT) with the Brownian motion (Brown, 1827) are used to determine the dispersion and advection of particles resulting from building demolition. Sutherland–Einstein Diffusion Analysis relies on the principles of the Einstein-Stokes equation and offers a robust framework for predicting the diffusion behavior of particles in a fluid environment. The Einstein-Stokes equation is expressed as:

$$D = \frac{kT}{6\pi\mu r} \tag{1}$$

where D is the diffusion coefficient, k is Boltzmann's constant, T is the absolute temperature, μ is the dynamic viscosity of the fluid, r is the radius of the particle. This equation shows the impact of temperature, viscosity, and particle size on diffusion. It demonstrates that, as temperature increases, the kinetic energy of particles increases, leading to greater diffusion.

While the Einstein-Stokes equation provides a fundamental understanding of diffusion, the objective is to obtain an accurate diffusion coefficient value tailored to the specific environmental and particle conditions under consideration. To achieve this, a calibration process integrating elements of Brownian motion modeling is employed.

Brownian motion describes the erratic, random motion of particles suspended in a fluid medium. This chaotic movement results from the continuous, random impacts of fluid molecules on the suspended particles. Mathematically, it is represented as:

$$MSD(t) = 2Dt \tag{2}$$

where $MSD(t)$ is the mean squared displacement at time t. Brownian motion serves as the fundamental behavior upon which diffusion analysis is constructed. It reveals how individual particles disperse unpredictably in a fluid due to thermal energy. Using the Brownian motion and Einstein-Stokes equation a calibration is conducted. The calibration process begins with the setup of essential parameters, including the

number of calibration steps, time interval, and the temperature of the system. Variables for the initial arbitrary diffusion coefficient, as well as the x and y coordinates for particle positions, are initialized. Brownian motion is simulated for each step within the defined calibration period. Random displacements for x and y are generated, and, in this description, fixed values are utilized in place of random functions. Particle positions are updated accordingly. The MSD is computed by comparing the particle's positions to their initial values for each time step. MSD data is fitted to a linear model using the least-squares method, resulting in a calculated slope. Finally, the calibrated diffusion coefficient is determined by dividing the slope by 4 times the temperature.

After finding the diffusion coefficient, the random walk particle tracking method, involving simulating the movement of particles in a fluid environment by incorporating both Brownian motion and advection effects, is employed. The mathematical description of RWPT is illustrated below.

$$x(t+\nabla t) = x(t) + \left(u + \frac{\partial D}{\partial x}\right)\nabla t + \sqrt{2D\nabla t}N(0,1) \tag{3}$$

$$y(t+\nabla t) = y(t) + \left(v + \frac{\partial D}{\partial y}\right)\nabla t + \sqrt{2D\nabla t}N(0,1) \tag{4}$$

where $x(t)$ and $y(t)$ represent the particle's position in the x and y directions at time t, ∇t is the time step, u and v are the velocity components in the x and y directions and $N(0,1)$ denotes random numbers drawn from a normal distribution with mean, 0 and standard deviation, 1.

To calculate the concentration of particles at different distances from the source, the Gaussian dispersion model is used. The Gaussian dispersion model is particularly useful for predicting the concentration of pollutants originating from point sources (Zhao et al., 2011), such as industrial emissions or in this case, the demolition of buildings following an earthquake. The model assumes that the dispersion of pollutants follows a Gaussian (normal) distribution in both the horizontal (crosswind) and vertical directions. The concentration of pollutants C at a given distance, x, from the source can be expressed using the Gaussian dispersion model as follows:

$$C(x,t) = \frac{Q}{2\pi u\sigma_y\sigma_z} exp\left(-\frac{x^2}{2{\sigma_y}^2}\right) exp\left(-\frac{x^2}{2{\sigma_z}^2}\right) \tag{5}$$

Where $C(x,t)$ is the pollutant concentration at distance x and time t, Q is the emission rate of pollutants from the source, σ_y is the horizontal standard deviation, which describes the dispersion of pollutants in the crosswind direction and σ_z is the vertical standard deviation, representing the vertical dispersion of pollutants. The first term on the right side of the equation represents the source emission rate and the dispersion coefficients, and the second and third terms describe the horizontal spread of pollutants with distance from the source and the vertical dispersion, respectively. A larger σ_y value corresponds to greater dispersion in the crosswind direction, whereas a larger σ_z value indicates a greater vertical spread. To smooth the concentration distribution, projection functions are applied, redistributing a portion of each particle's mass to adjacent grid cells (Moeller and Adams, 1993; Bagtzoglou et al., 1992).

The experimental data of a study carried out for dispersion in urban regions (Venkatram et al., 2004) is utilized to compare the used model. The derived concentrations from the measurements taken at specific distances (200 m, 500 m, 1000 m, and 2000 m) from a regional source, which is an industrial area, are presented in Fig. 1, along with the results from the dispersion model used in this study. There is no data on the origin of the dust source. Therefore, the concentration data given for 200 m is used for normalization of the whole data set. While there are some differences between the experiment and the model, it is not the aim of this research to determine the exact amount of dust concentration at every distance. The purpose is to make a comparison between concentration amounts. Changing circumstances can alter the concentration

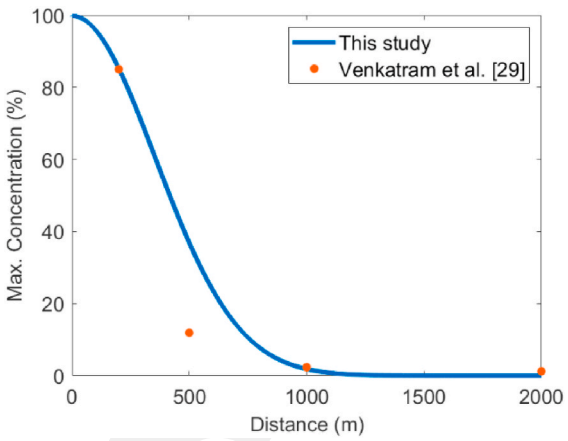

Fig. 1. Max concentration with respect to distance.

levels in the region, but it is assumed that all areas have the same conditions. Therefore, the result of intercomparison remains consistent regardless of the changing conditions.

2.2. The AHP

The Analytical hierarchy process (AHP) is the most popular method (Demir and Dinçer, 2023; Dinçer et al., 2023; Demir et al., 2023; Yılmaz et al., 2023) among the multi-criteria decisioning methods. It is applied to many different areas (Rahmat et al., 2017; Rekik and El Alimi, 2023). Irrespective of the applied area, AHP results define the weights of the specified criteria. The weights are needed as a decision parameter for predefined functions or decision limits. For a reliable decision given by AHP analysis (Demir et al., 2024), the criteria and interrelations of criteria should be specified correctly. The interrelations compose a matrix of which elements define the relations of the criteria couples. The step of composing the interrelation matrix couple by couple is done mostly by experts' opinions. Then, the interrelation matrix is normalized by dividing each element by the column-wise summation, and the row-wise means of the resulting matrix are computed. These row-wise means represent the weights assigned to each criterion. The summation of weights of criteria should be 100%. Finally, the weights can be used for decisions which are mostly a ranking or limiting factor.

The AHP uses a consistency ratio, which is a measure of how much the judgments deviate from being perfectly consistent. A consistency ratio close to zero indicates a high level of consistency, while a higher ratio suggests greater inconsistency. The equations to calculate the consistency ration are:

$$CI = \frac{\lambda_{max} - n}{n-1} \tag{6}$$

$$CR = \frac{CI}{RI} \tag{7}$$

Where CI is the consistency index, λ_{max} is the principal eigenvalue of the interrelation matrix, n is the order of the matrix, RI is the Random Index, a constant value based on the matrix order and CR is the consistency ratio. A small CR indicates good consistency. As a rule of thumb, if CR is less than 0.1, the consistency is considered acceptable.

2.3. The algorithm

The wind speed and direction vary monthly and even daily worldwide, so the affected regions of dust from a demolition site change. This is because dust dispersion depends on the wind's direction and speed. To identify the affected regions for each time period, a GIS-based analysis is essential. This analysis, carried out through pixel-by-pixel analysis using

MATLAB, determines the coordinates of the dust-affected region by applying a dispersion model to a demolition site with known wind speed and direction. It is similar to the wake effect analysis of wind turbines carried out in wind farm layout optimization studies (Demir et al., 2024; Patel et al., 2017; Dinçer et al., 2024).

Depending on the size of the demolition site and spatial constraints such as urban spaces and land use across the entire region, it is necessary to divide large and discontinuous/nonuniform demolition sites into subsites. In essence, the entire demolition site is represented by several subsites (where " *noss* " denotes the number of subsites). This allows for the determination of the optimal demolition time period for each subsite by conducting the necessary calculations individually for every subsite.

By analyzing the maximum dust concentration rates on each neighboring pixel affected by dust on the map, the exposure rate matrix for a demolition subsite, ${}^{exp}D^{ss}(i,j,m)$, is achieved where i and j represent coordinates, m represents the time period, and ss corresponds to the demolition subsite. For each subsite, it is essential to establish a defined demolition period. In the proposed method, the demolition period for each subsite is specifically defined as a month-long duration.

The exposure rate matrix characterizes the maximum dust exposure rate for each pixel within the demolition subsite, determined by monthly wind speed and direction (with a rate ranging from 0% for minimum exposure to 100% for maximum exposure). Several assumptions underpin the feasibility of the study. Firstly, a constant wind speed and direction throughout the given month is assumed, implying a continuous flow from the prevailing wind direction. In turbulent flow, dust particles exhibit transverse motion in the air, defined stochastically by eqs. (3) and (4). The maximum exposure rate on a pixel is considered as its exposure rate, taking into account that not every pixel within a subsite is demolished simultaneously. Each neighboring pixel is exposed to dust for a constant time period as defined in eqs. (3) and (4), but the exposure rate varies for each neighbor pixel according to eq. (5). Assuming that the amount of dust spread from each subsite is constant, using the maximum dust exposure rate on a pixel is more representative to define the exposure rate. Although a CFD-based analysis is recognized as an accurate solution for representing dust exposure on each neighbor pixel (Kuo et al., 2016; Demir, 2020; Demir et al., 2021; Dinçer, 2020; Velioglu et al., 2015), it is deemed impractical for a site defined with high resolution.

The dust exposure rate alone does not provide insight into the impact on humans or the environment due to variations in urban spaces and environments across the region. To account for these differences, a vulnerability map is essential to identify the sensitivity to dust in the specified region. The process involves defining necessary criteria for the given region, which are then weighted using the AHP method to establish their relative sensitivities to dust exposure. Subsequently, the vulnerability map $V(i,j)$ is generated through ArcGIS, incorporating the defined interrelated criteria. It's important to note that this map remains constant over time, as the specified criteria do not change throughout the year.

To calculate the dust effect rates ${}^{eff}D^{ss}(i,j,m)$ across the selected region, an element-by-element multiplication of matrices, representing exposure rates and vulnerabilities, as outlined in eq. (8), is employed. This effect rate matrix delineates the pixel-specific impact of dust emanating from a demolition subsite on a monthly basis. Consequently, the dust effect rate is determined by considering both the exposure to dust and the vulnerability to dust. It's important to note that in eq. (8), both matrices being multiplied consist of percentages.

$$eff_{D^{ss}}(i,j,m) = exp_{D^{ss}}\backslash(i,j,m) \bigodot V(i,j) \tag{8}$$

The dust effect rate matrix illustrates the impact rate for each pixel on the map. However, to facilitate comparisons between demolition months for a specific subsite or even among all subsites, a scalar effect rate is required. The monthly scalar dust effect rate is defined as the summation of ${}^{tot}D^{ss}_{m}$, as outlined in eq. (9). This summation aggregates the rates of dust effect on each pixel, providing the total dust effect for a subsite.

It's important to note that the total dust effect, ${}^{tot}D^{ss}_{m}$, is influenced by the shape and size of the subsite. For instance, a small subsite results in a small dust-affected region, and vice versa. Additionally, the dust-affected region is smaller for a subsite with a slender profile in a direction perpendicular to the prevailing wind, while it is larger for a thicker subsite in the same direction. Briefly, the total dust effect is proportional to the size and shape of a subsite. In other words, the dust effect should be represented irrespective of the size and shape of a subsite. Instead, it should represent the dust effect for a unit dust nozzle.

$${}^{tot}D^{ss}_{m} = \sum_{i=1}^{nor}\sum_{j=1}^{noc} {}^{eff}D^{ss}(i,j,m) \tag{9}$$

Where the number of rows in the matrix is *nor* and the number of columns in the matrix is *noc*.

The hydraulic diameter serves as a size representation for a nozzle, independent of its shape. In the context of treating a subsite as a dust nozzle, it becomes more meaningful to use the hydraulic diameter of the subsite, denoted as $\mathit{Ø}^{ss}_{hyd}$, to define the unit dust effect for each site, represented as ${}^{un}D^{ss}_{m}$. In eq. (10), the total dust effect of each subsite is divided by its corresponding hydraulic diameter, resulting in the unit dust effect for each subsite. To elaborate, the process of determining ${}^{un}D^{ss}_{m}$ for each subsite and month is detailed in a flowchart presented in Fig. 2.

$${}^{un}D^{ss}_{m} = {}^{tot}D^{ss}_{m} \Big/ \mathit{Ø}^{ss}_{hyd} \tag{10}$$

To facilitate comparisons between different months or subsites, it is essential to determine the unit dust effect for each demolition subsite in every month, denoted as ${}^{un}D^{ss}_{m}$. Conducting an intermonth comparison of unit dust effects for a specific subsite enables the establishment of a priority rank. The month corresponding to the minimum unit dust effect value for a given subsite, M^{ss}, is identified as the optimal month for the demolition of that subsite, as outlined in eq. (11).

$${}^{un}D^{ss}_{M^{ss}} = \min_{1\le m\le 12} {}^{un}D^{ss}_{m} \tag{11}$$

The ideal scenario for the demolition plan involves carrying out the demolition of each subsite during its optimal month, M^{ss}. However, the feasibility of this approach hinges on the availability of the required staff and equipment. Given that multiple subsites may have their respective optimal demolition months, it becomes crucial to consider the necessary duration for the total demolition activity, reflecting the contract due date. This duration is instrumental in determining the requisite number of staff and equipment.

Therefore, there are three plausible scenarios for the demolition plan. The first scenario entails demolishing each subsite in its best month and subsequently calculating the needed number of staff and equipment accordingly. On the other hand, the second scenario involves determining the necessary number of staff and equipment to complete the demolition of all subsites within the contracted due date. In this scenario, the focus is on identifying the least impactful demolition subsite to be prioritized for each month, especially when the region to be demolished is constrained. In the third scenario, maximization of the gain of selection of a site for demolition in a given period is the objective function.

The scheduling for the first demolition scenario is straightforward, involving the identification of optimal demolition months for each subsite as outlined in eq. (11). Conversely, this approach cannot be employed for scheduling in the second plan. In the second plan, the scheduling is determined by specifying the absolute minimum unit dust effect, denoted as ${}^{un}D^{ss^*}_{M^{ss^*}}$ which represents the least impactful scenario across all months and subsites, as detailed in eq. (12).

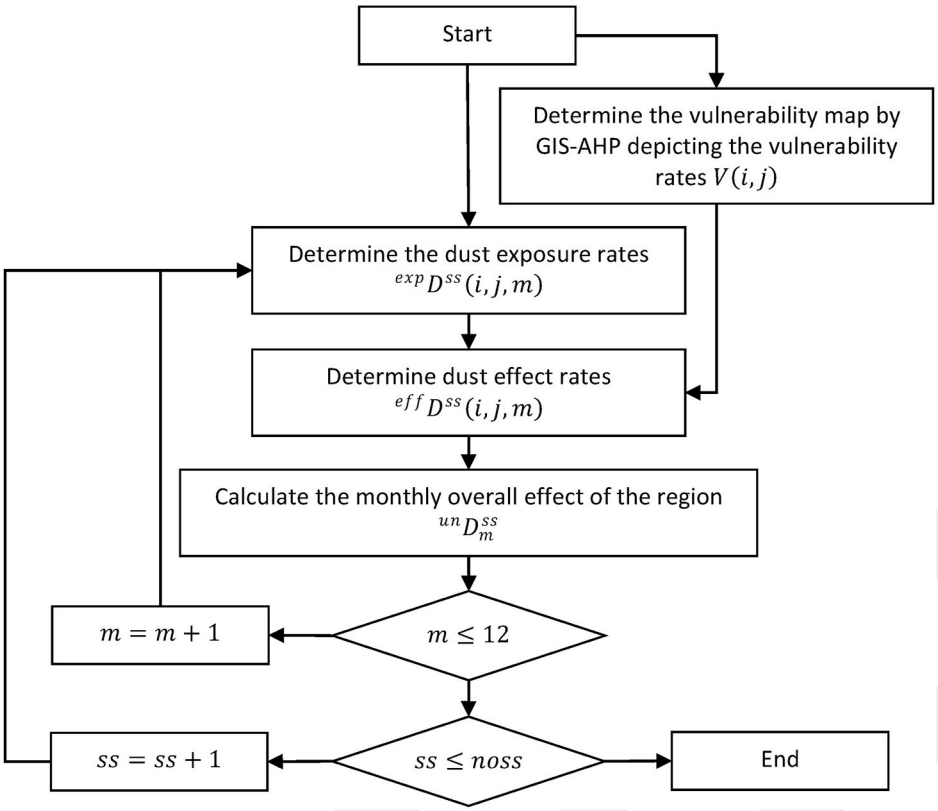

Fig. 2. Flow chart for determining minimum effect of a demolition region.

$$ {}^{un}D_{M^{ss^*}}^{ss^*} = \min_{1\leq ss\leq noss}\left(\min_{1\leq m\leq 12} {}^{un}D_m^{ss}\right) \tag{12}$$

The absolute minimum unit dust effect, ${}^{un}D_{M^{ss^*}}^{ss^*}$, indicates the subsite to be demolished, ss^*, and its corresponding demolition month, M^{ss^*}. Assuming that each demolition site can be demolished within a month, a schedule can be systematically constructed by specifying the ${}^{un}D_{M^{ss^*}}^{ss^*}$ after each assignment of a subsite to a specific month.

Another optimal solution (third scenario) is designed based on the absolute maximum gain satisfied by selecting the cleaner way of demolition as defined in eq. (13). The absolute maximum of the difference between the average normalized unit dust effect of a subsite and the normalized unit dust effect is the gain for a cleaner demolition schedule. Assuming that each demolition site can be demolished within a month, a schedule can be systematically constructed by specifying the ${}^{un}D_{M^{ss^{**}}}^{ss^{**}}$ after each assignment of a subsite to a specific month.

$$ {}^{un}D_{M^{ss^{**}}}^{ss^{**}} = \max_{1\leq ss\leq noss}\left(\max_{1\leq m\leq 12}\left(\frac{\sum_{m=1}^{12} {}^{un}D_m^{ss}}{12} - {}^{un}D_m^{ss}\right)\right) \tag{13}$$

The choice between the three scenarios depends on the specific circumstances of the demolition project. Opting for the second and third scenario are advisable when the demolition is contractually bound by a due date. On the other hand, the first scenario may be preferable if the duration of the demolition period is a limiting factor or if it is practical to assemble the required team. In the second and third scenario, a dedicated team equipped with the necessary tools and vehicles operates throughout the contracted period. This team efficiently transitions the equipment and vehicles to the next demolition site as the month changes, ensuring that the overall demolition activity is completed within the specified due date. Two additional scenarios are composed to depict the limits dust effect and compare them. However, the fourth and fifth scenarios do not have any objective function as defined for first three scenarios (see eqs. (11)–(13)).

2.4. Study area

The proposed methodology is implemented in the city center of Kahramanmaraş (refer to Fig. 3), chosen as the focal area for this study. This location is deemed ideal for showcasing the effectiveness of the methodology, given the recent destructive earthquake that occurred on February 6, 2023 (Dinçer et al., 2024). The province currently requires a demolition schedule, while the remnants of the damaged structures are presently being transported to temporary recycling sites (Demir and Dinçer, 2023).

A report published by the Republic of Türkiye Ministry of Environment, Urbanization and Climate Change provides a detailed assessment of the region, revealing that there are 11,984 risky buildings in Kahramanmaraş city center which is 3017 km^2. There are 68 schools, 13 hospitals, and 30 temporary shelters to take care of dust spread out from demolition of damaged buildings. Given these circumstances, Kahramanmaraş urgently requires an efficient demolition plan (refer to Fig. 4). Therefore, the province stands out as the most suitable location to demonstrate the advantages of the proposed methodology.

As indicated, there are many buildings to be demolished on the site and buildings are not identical. The type and height of buildings are primarily influenced by the municipality's development plan. Moreover, damaged buildings are concentrated in specific areas, such as those that have collapsed. Consequently, thorough inspections and studies are imperative on the site to categorize it into subsites, each generating a comparable amount of dust. The authors delineate these subsites, as illustrated in Fig. 5, based on their site investigations.

Table 1 provides the annual wind speeds and directions. Monthly data on wind speeds and directions are necessary for the implementation of the proposed methodology. The prevailing wind directions in Table 1 are expressed in degrees, following a clockwise direction starting from the north. It is assumed that the wind characteristics remain constant for

Fig. 3. Kahramanmaraş city center.

Fig. 4. Destruction in Kahramanmaraş due to earthquake on 6th February of 2023.

each monthly period, providing a defined scope for the research context.

3. Results

While the concept of dust vulnerability rating is universal, specific site characteristics can introduce variations. In earthquake-damaged regions, temporary shelters coexist with vulnerable locations like airports, schools, and hospitals. Considering these regional characteristics, an AHP analysis is conducted, and the results are presented in Fig. 6. By assigning the AHP findings into a map using a color spectrum, a vulnerability map is created, illustrating the vulnerability of each pixel in Kahramanmaraş city center. Figure 7 depicts this map, where the most vulnerable sites are highlighted in dark red, while less vulnerable areas are represented in light red and colorless. It's important to note that the demolition subsites include residential areas, and as the demolition schedule is unknown before the analysis, these subsites are assumed to also encompass residential zones.

To calculate the dust effect rates for each pixel on the map, the dust exposure rate is essential, as indicated in eq. (8). The dust exposure in a specific region relies on both the defined dispersion model, which

Fig. 5. Demolition sub-sites.

Table 1
Monthly wind speeds and directions for Kahramanmaraş city center.

Month	Speed (m/s)	Direction (Deg)
January	2.86	229
February	2.92	219
March	2.89	162
April	2.83	121
May	2.89	123
June	3.50	128
July	3.75	130
August	3.47	126
September	3.03	124
October	2.61	163
November	2.58	214
December	2.75	233

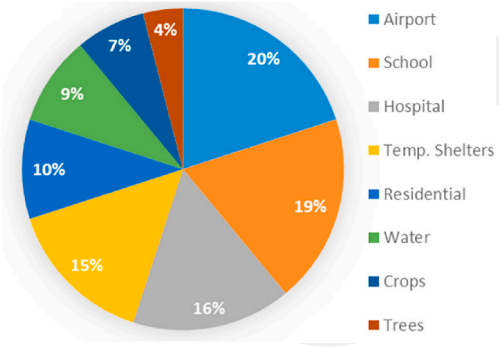

Fig. 6. Weights of criteria.

determines particle concentrations in the air by the wind characteristics. Wind characteristics, including prevailing wind speed and direction for the city center of Kahramanmaraş, are detailed in Table 1. By incorporating the dispersion model and monthly wind characteristics, dust exposure maps for each subsite are generated for every month.

By multiplying the vulnerability matrix with the dust exposure matrix, dust effect matrices, which represent the dust effect values of each pixel on the map, are obtained for each subsite every month. For instance, Fig. 8 illustrates the annual dust effect map for demolition subsite F, derived by processing the ${}^{eff}D^{F}(i,j,m)$, onto the map. However, as these are matrices, direct comparison is challenging. To enable intercomparison among months and subsites, unit dust effect rates, ${}^{un}D^{F}_{m}$, (scalar numbers) are calculated for each subsite per month using eq. (10). This step is crucial as scalar representations of the dust effect matrices are needed. The normalized unit dust effect rates are then summarized in Table 2 in which normalized values of ${}^{un}D^{F}_{m}$ can be seen in column F. establishing an interrelation between the unit dust effect rates of each subsite and month. Table 2 contains normalized values of dust effect rates of all subsites for all months. This table has all needed data to construct a demolition plan.

Table 2 displays the unit dust effect rates of all subsites for every month. To provide a comparison of subsites, Table 2 is shown as graphs in Fig. 9. These graphs reveal that the unit dust effect rates of each subsite are similar to the monthly wind speed of the Kahramanmaraş province. This is because dust effect rates are derived from dust exposure rates, which are directly linked to the speed of wind, as defined in eqs. (3) and (4). If all subsites had the same hydraulic diameter and a homogeneous vulnerability region throughout the entire province, then they would all have the same unit dust effect rate. However, the hydraulic diameter of the subsites and the vulnerability around subsites vary, which causes differences in the unit dust effect. The level of unit dust effect rate is influenced by the hydraulic diameter of the subsite. Additionally, the variation in rates throughout the year is due to the non-uniform vulnerabilities surrounding the subsite. This is because the direction of the prevailing wind changes throughout the year, causing the affected region to change with the wind's direction.

4. Scenarios

Five scenarios are developed to observe the limits of dust effect and compare the demolition plans. The first plan places the highest priority on minimizing the dust impact on individual units. The second and third plan strives to achieve the optimal dust effect per unit based on different objective functions. The fourth plan prioritizes contractor efficiency, overlooking pollution concerns. Finally, the fifth plan, designed as a worst-case scenario, is formulated to evaluate the effectiveness of the other demolition schedules. Table 2, which consists of unit dust effect rates of all subsites for all months, has all the data needed to construct any demolition plan. The first three scenarios are composed based on eqs. (11)–(13), respectively. In contrast, the last two scenarios have no

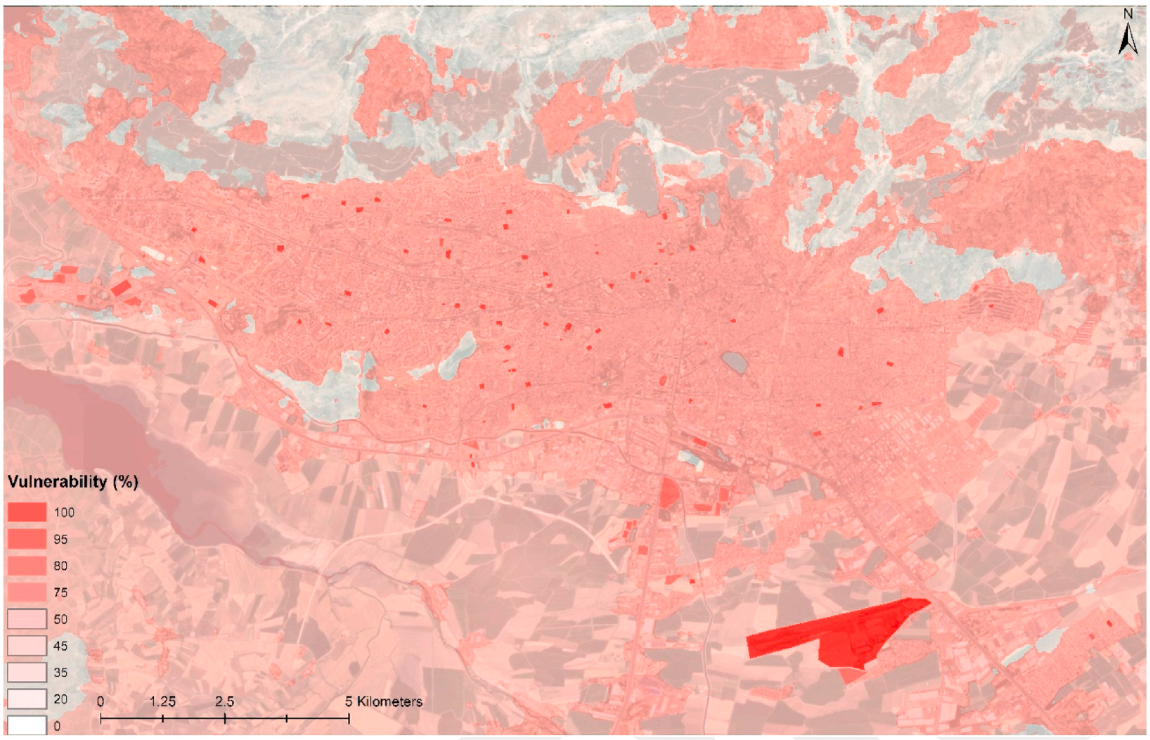

Fig. 7. Vulnerability map of Kahramanmaraş city center.

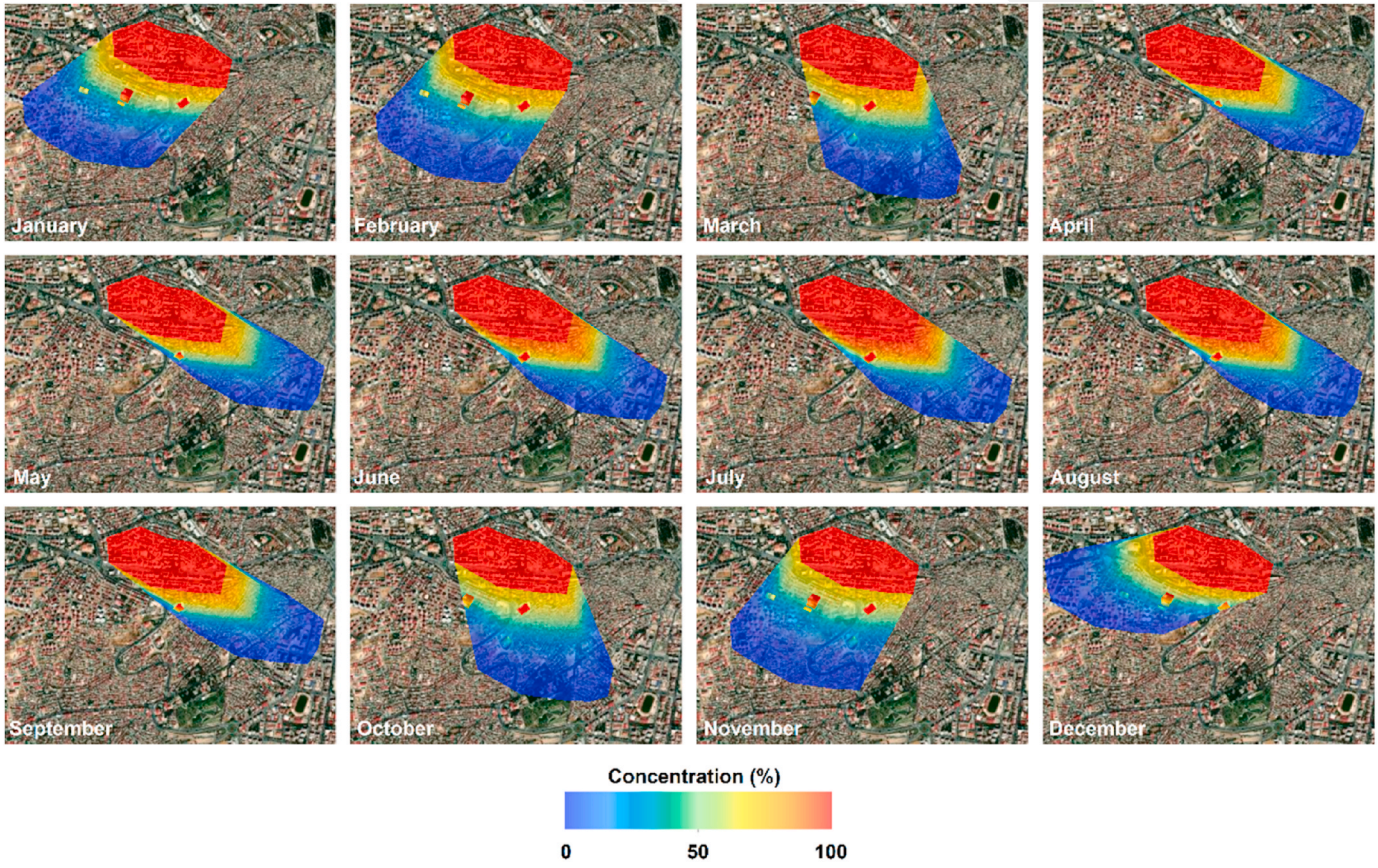

Fig. 8. Annual dust effect rate map of demolition subsite F.

Table 2
Normalized unit dust effect rates.

Month	A	B	C	D	E	F	G	H	I
January	0.37	0.42	0.46	0.39	0.36	0.44	0.75	0.55	0.49
February	0.40	0.44	0.45	0.39	0.37	0.46	0.82	0.58	0.50
March	0.41	0.46	0.43	0.36	0.34	0.43	0.86	0.58	0.48
April	0.29	0.41	0.48	0.34	0.31	0.36	0.70	0.55	0.43
May	0.31	0.42	0.48	0.35	0.32	0.37	0.73	0.56	0.44
June	0.39	0.51	0.57	0.43	0.38	0.46	0.91	0.67	0.53
July	0.43	0.56	0.62	0.47	0.42	0.50	1.00	0.72	0.58
August	0.38	0.50	0.57	0.42	0.38	0.45	0.89	0.67	0.52
September	0.33	0.44	0.51	0.37	0.33	0.39	0.77	0.59	0.46
October	0.37	0.41	0.39	0.32	0.31	0.39	0.78	0.52	0.44
November	0.36	0.40	0.39	0.34	0.33	0.41	0.75	0.52	0.44
December	0.33	0.40	0.48	0.38	0.33	0.39	0.57	0.52	0.43

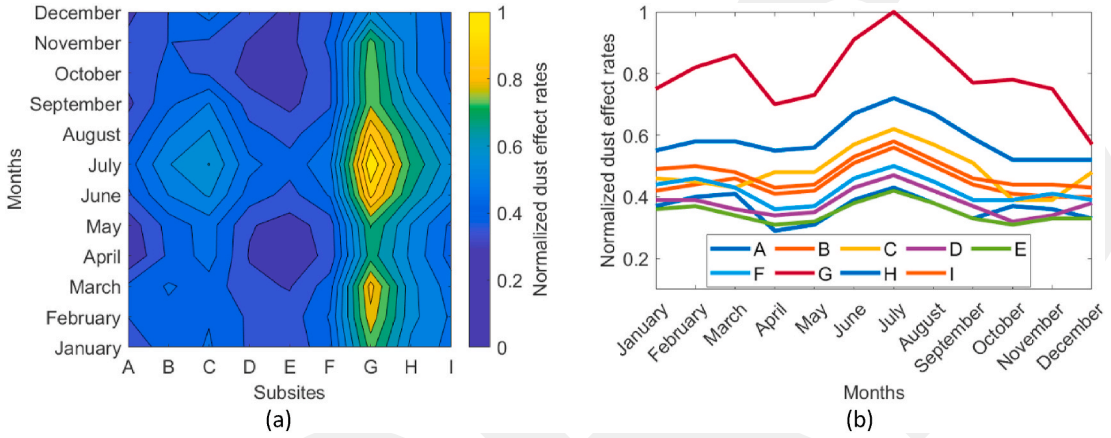

Fig. 9. Graphical illustration of normalized unit dust effect rates as contour (a) and line (b).

objective function.

5. Scenario 1

In the first scenario, the government mandates a demolition schedule to the contractor with the objective of minimizing the dust impact based on eq. (11). It is assumed that the contractor possesses the necessary equipment to carry out the demolition of each subsite during the month, which results in the least dust dispersion. However, prior to analysis, it is uncertain whether all subsites exhibit the minimum dust effect simultaneously or if the months of minimal dust effects vary for each subsite. To determine the optimal demolition months for each subsite, specifying the minimum dust effect rates throughout the year is necessary. This enables the identification of the demolition months for each subsite, facilitating the determination of the required equipment and team allocation. The resulting demolition months causing the minimum dust effect for each subsite are presented in Table 3.

Table 3 reveals that multiple subsites are scheduled for demolition during the same months. Consequently, the contractor must be equipped to demolish four subsites simultaneously. In this scenario, the workload is not continuous throughout the contract period, with breaks occurring in January, February, March, May, June, July, August, September, and October. Even if the demolition commences in November, the demolition teams are required to take a three-month break in January, February, and March. The scenario envisions the completion of demolition by the end of April. The dust effect map for the first scenario is shown in Fig. 10.

In Table 4, the normalized unit dust effect rates, with a mean of 0.40, are provided for each subsite. According to these normalized rates, the first scenario results in a unit dust effect rate that is 40% of the unit dust effect expected during the demolition of subsite G in July, which, as indicated in Table 2, yields the highest unit dust effect among all subsites.

6. Scenario 2

In the second scenario, the government mandates a demolition schedule where each subsite is to be demolished in a different month. Consequently, the contractor must be adequately equipped to demolish a subsite within a single month. The determination of the demolition month for each subsite follows a systematic selection process. The month chosen for demolition is based on identifying the absolute minimum unit dust effect, as defined in eq. (12). The demolition months for all subsites are determined by specifying the absolute minimum unit

Table 3
Schedule of the scenarios.

Scenario	Jan.	Feb.	Mar.	Apr.	May	Jun.	Jul.	Aug.	Sep.	Oct.	Nov.	Dec.
1				F, A, E, I							C, D, H	B, G
2	H	G	C	A	F				I	E	D	B
3	B	E	D	A	F				I	C	H	G
4			G	F	C	B	A	D	E	H	I	
5							All					

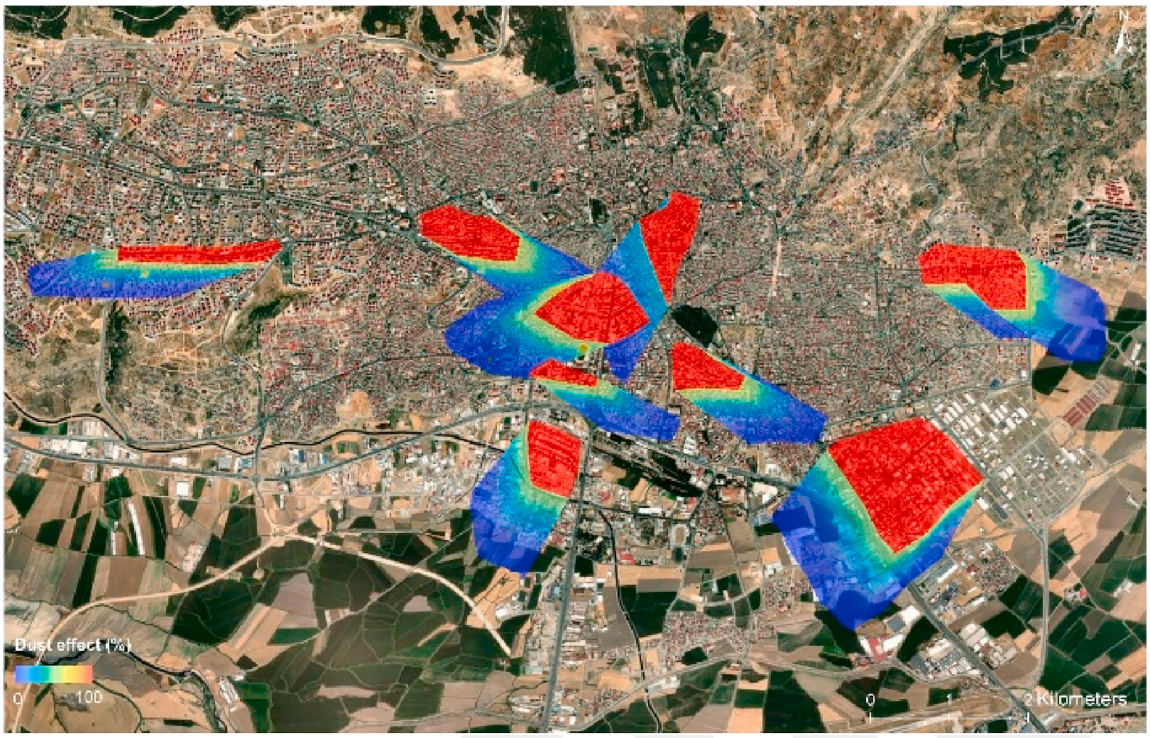

Fig. 10. Dust effect map of scenario 1.

Table 4
Dust effect rates of scenarios.

Scenario	A	B	C	D	E	F	G	H	I	Mean
1	0.29	0.40	0.39	0.34	0.31	0.36	0.57	0.52	0.43	0.40
2	0.29	0.40	0.43	0.34	0.31	0.37	0.82	0.55	0.46	0.44
3	0.29	0.42	0.39	0.36	0.37	0.37	0.57	0.52	0.46	0.42
4	0.43	0.51	0.48	0.42	0.33	0.36	0.86	0.52	0.44	0.48
5	0.43	0.56	0.62	0.47	0.42	0.50	1.00	0.72	0.58	0.59

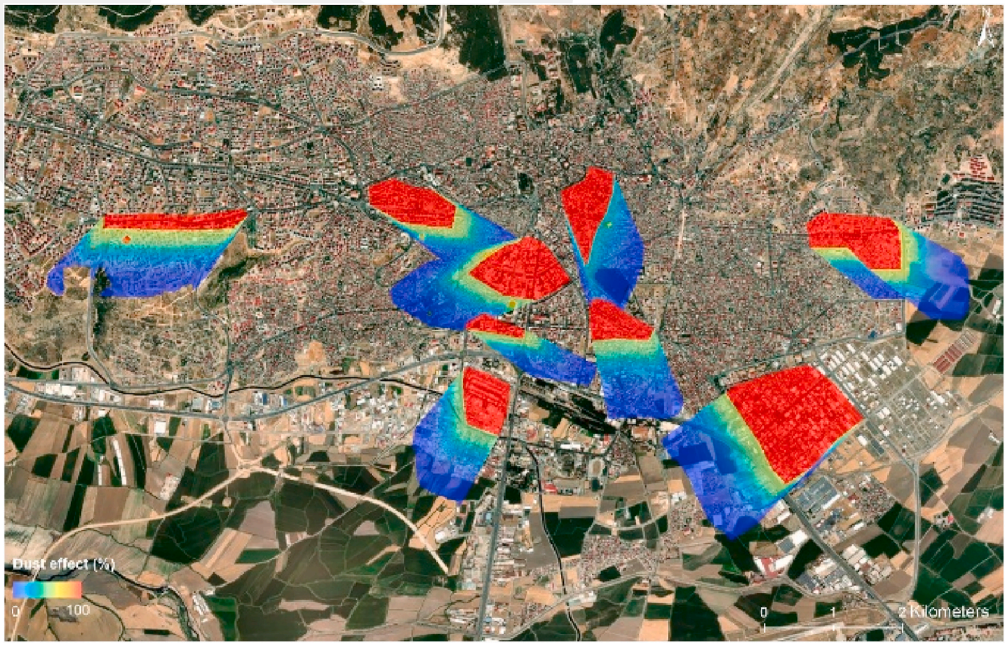

Fig. 11. Dust effect map of scenario 2.

dust effect after each demolition month. This approach results in a schedule, outlined in Table 3, which optimally minimizes the unit dust effect on both human health and the environment.

According to the prescribed schedule, the contract is scheduled to commence in September and conclude at the end of May. Unlike the first scenario, where the contract spans 8 months with nonuniform demolition activity, the second scenario envisions a uniform demolition activity. In this context, it is observed that the summer season is deemed the least favorable for demolition activities. This is attributed to summer being the windiest season, leading to an increase in dust concentrations in the air. The corresponding dust effect map is presented in Fig. 11.

The mean of the unit dust effect rates for subsites in the second scenario is calculated to be 0.44 (refer to Table 4). As anticipated, the mean unit dust effect rate in the second scenario is higher than that in the first scenario. This discrepancy arises because, while the first scenario is designed based on the selection of absolute minimum unit dust effect rates for each subsite, the second scenario is composed according to optimal minimum unit dust effect rates. The optimality condition is defined by the requirement for uniformity in the demolition activity throughout the specified contract period.

7. Scenario 3

This scenario aims to demonstrate the significance of using the right objective function for optimal solutions. The optimality function used in this scenario is composed to increase the gain obtained by the difference between the average unit dust effect of the subsite and the unit dust effects of that site throughout the year. By satisfying the maximality of the objective (see eq. (13)), the total unit dust effect of the scenario is minimized. The results show that a solution that is 5% better than the second scenario is achieved (see Table 4). Furthermore, a closer result to the first scenario, which represents the absolute minimum, is obtained. The scenario is given in Table 3. The Corresponding dust effect result is visualized in Fig. 12.

8. Scenario 4

This scenario is developed under the assumption that the government does not mandate a specific demolition activity schedule for the contractor. Consequently, the contractor has the autonomy to plan the schedule, prioritizing the primary objective of minimizing expenses. While the primary cost for the contractor is associated with the demolition activities, an additional transportation cost arises due to the specific locations of subsites within the city center. After completing a subsite, vehicles must be transported to the next demolition location. Although this transportation cost is relatively small compared to the expenses of demolition activities, the unconstrained contractor would prefer to move the demolition vehicles and teams to the nearest subsite. The contractor actively plans the demolition activities to minimize transportation, aiming for a seamless flow without interruptions. Any pause in the demolition activity incurs additional expenses for the contractor. Thus, the contractor aims to spread the demolition activity over the contract period to avoid unnecessary labor expenses.

Furthermore, if the contract does not dictate a specific start date, the contractor prefers the warm season for the demolition activity. This choice is motivated by the desire for more favorable working conditions and increased employee productivity during warmer weather.

In the fourth scenario, the contractor formulates the demolition plan to minimize transportation expenses based on the distances between neighboring subsites, as outlined in Table 5. The resulting schedule is presented in Table 3, and the corresponding unit dust effect rates are provided in Table 4. Based on the defined demolition schedules, the total transportation distances are calculated as 28.7 km, 32.7 km, 31.4 km, and 20.6 km for scenarios 1, 2, 3, and 4, respectively. The contractor aims to minimize the total vehicle transportation distance in the city center, with the minimum value set at 20.6 km. The dust effect map for this scenario is shown in Fig. 13.

Table 5
Distance to neighbor subsite in meter.

Subsite	B	C	D	E	F	G	H	I
A	973	2270	1110	1770	2100	4800	4700	5600
B		1385	2000	1550	1890	5100	4560	5100
C			3300	1740	2600	6125	4400	4000
D				2150	3000	5300	4500	6000
E					3400	6600	3000	3900
F						3500	6400	6500
G							9600	9900
H								2750

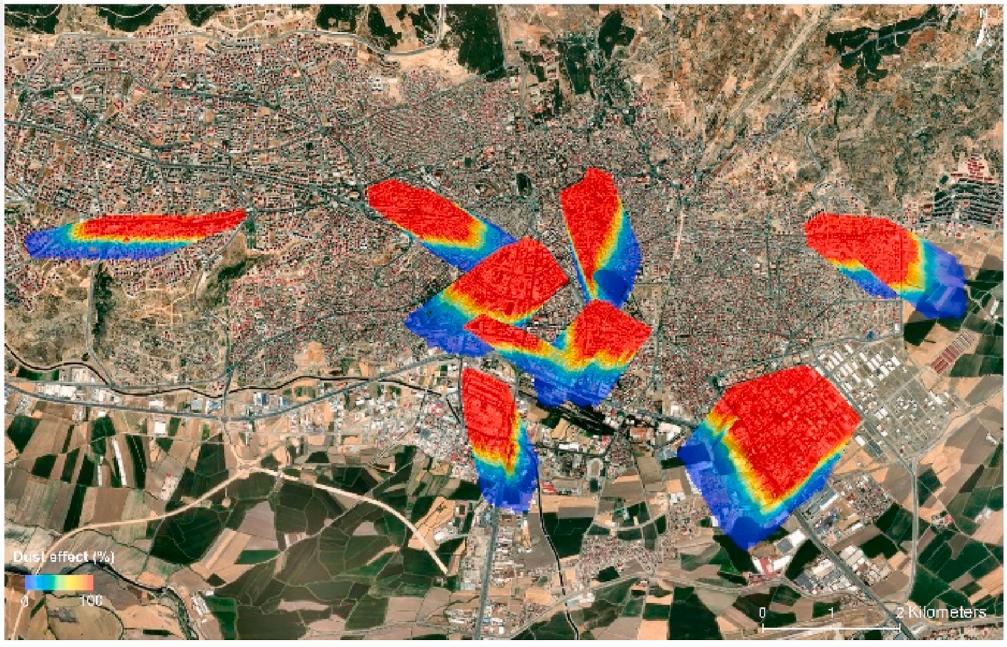

Fig. 12. Dust effect map of scenario 3.

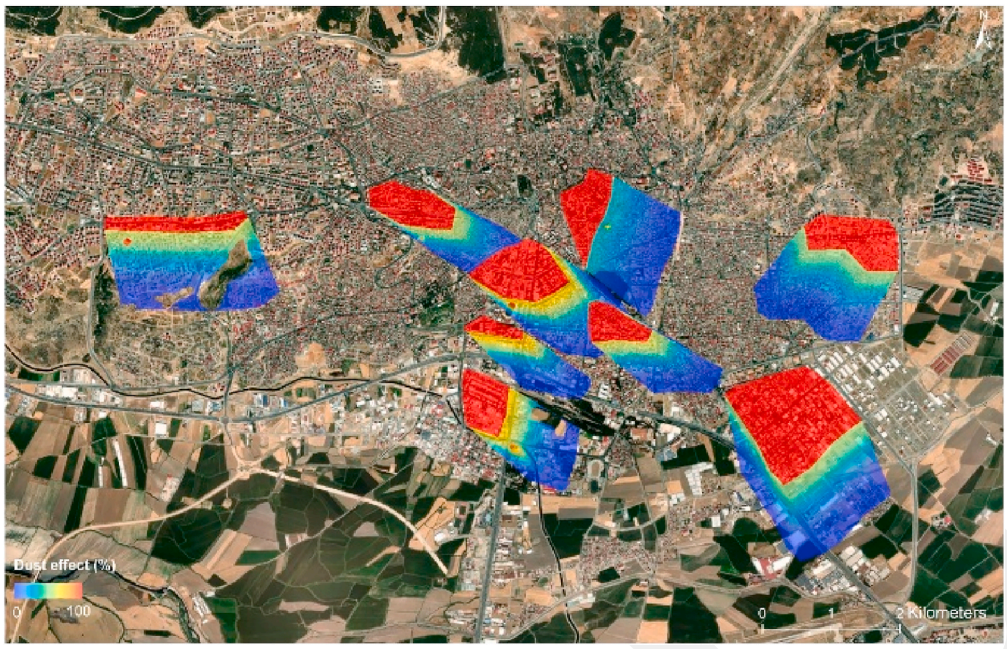

Fig. 13. Dust effect map of scenario 4.

9. Scenario 5

The fifth scenario is designed as the worst-case scenario, intended to illustrate the extent of mitigation of dust effects. In this scenario, the contract period is not predetermined, and the demolition schedule is established by selecting the maximum normalized dust effect rates for the demolition month of each subsite. Examination of Table 2 reveals that the maximum normalized dust effect rate for every subsite occurs in July. Consequently, the schedule for the fifth scenario straightforwardly involves demolishing all subsites in July, resulting in a mean unit dust effect rate of 0.59. It's important to note that July is identified as the windiest month. Consequently, engaging in demolition activities during July leads to heightened dust concentrations in the air, rendering it the least favorable month for demolition. Despite this, the fifth scenario intentionally adopts this unfavorable condition to demonstrate the maximum potential dust impact, emphasizing the significance of mitigation efforts in other scenarios. Figure 14 presents the corresponding dust effect map.

10. Discussion of results

Project management is crucial for demolition activities (Liu and Pun, 2004). As there are many government regulations in place for demolition contracts (Demolition Work Plan FOR), safety should be the top priority (Alipour-Bashary et al., 2021). A clean and well-regulated plan is necessary, as unexpected contract terminations can occur due to environmental and health concerns. For instance, a demolition project was halted due to its negative impact on the health of surrounding

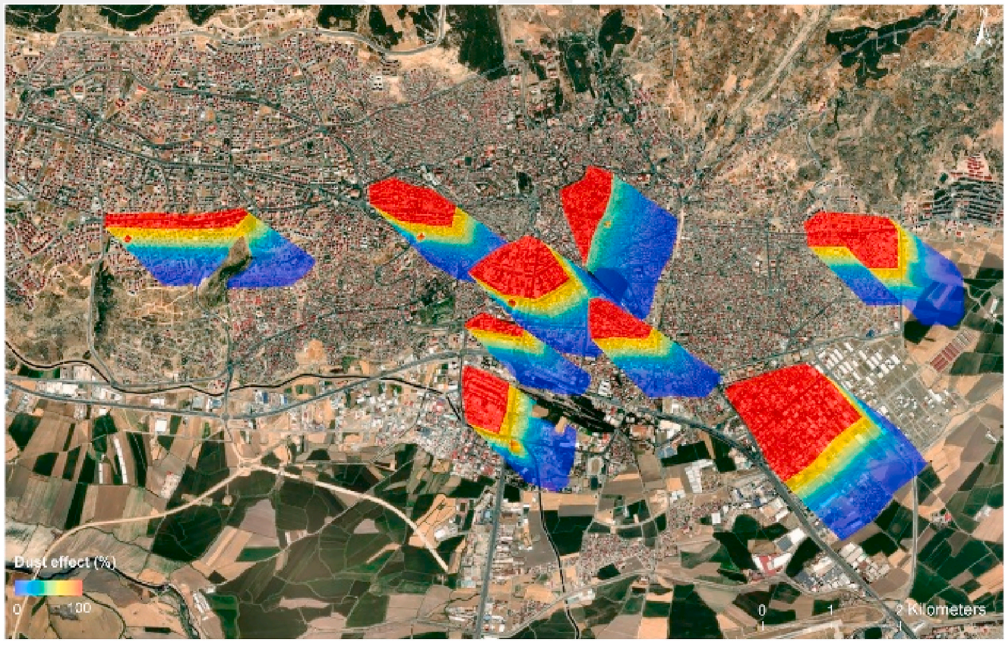

Fig. 14. Dust effect map of scenario 5.

residents (Chu, 2008). Such terminations can lead to additional costs for the government besides the environmental and social impacts.

In research conducted for the evaluation of the social sustainability of demolition (Yu et al., 2017), health and safety are evaluated as the third important issue even in terms of social impacts. Although activity time periods are directed by governmental regulations to mitigate the impact of noise pollution, there is no regulation for demolition schedules. A demolition schedule should be regulated by the government to mitigate the impact of dust exposure.

The impact of dust exposure (dust effect) resulting from building demolition is primarily influenced by wind characteristics and the vulnerability rates of the site. The definition of unit dust effect rates for demolition subsites enables a comparative analysis among subsites and demolition months. Consequently, it becomes possible to compose demolition schedules with known interrelated unit dust effect rates.

In order to showcase the mitigation of the impact of dust exposure, five distinct demolition schedules are devised as summarized in Table 6. The first schedule prioritizes achieving the absolute minimum unit dust effect, while the second and third aim for optimal unit dust effect utilizing different objective functions. The fourth schedule is constructed with a focus on contractor expediency, neglecting pollution concerns. Lastly, the fifth schedule, representing the worst-case scenario, is created to assess the effectiveness of the other demolition schedules.

The first schedule indeed results in the expected minimum unit dust effect rate. However, implementing this schedule requires the contractor to have a sufficient number of teams to complete the demolition. Moreover, the overall contract amount is anticipated to be higher due to nonuniform demolition activity or mandatory breaks defined in the schedule.

In an effort to reduce the contract amount by implementing a uniform demolition activity, the second and third demolition schedules are proposed. These schedules satisfy the uniformity of the demolition activity, but spreading the demolition over the contract period with a constant number of teams leadding. Based on the optimality equations of 2 & 3, an optimal solution can converge to the average unit dust effect of the first schedule, which is the absolute minimum dust effect case. The second and third schedules utilize different objective functions as seen in Table 6. Therefore, the average unit dust effects of scenarios 2 and 3 are not the same but close to scenario 1. Nevertheless, compared to an unscheduled demolition activity (fourth schedule) where the contractor is not obliged to adhere to any specific schedule, the second and third schedules achieve optimal unit dust effect rates, resulting in 8% and 13% reduction in dust effect, respectively.

For comparison purposes, a hypothetical worst-case scenario is constructed, although it is not realistic to carry out. The comparison reveals a significant difference in unit dust effect rates. The fifth scenario is 40% worse than the third scenario and even 48% worse than the first scenario, underscoring the importance of adopting effective demolition schedules to mitigate impact of atmospheric concentrations of deleterious particles.

Table 6
Differences and similarities of scenarios.

Scenario	Contract Details	Government Need	Optimality Equation	Freedom Level of Contractor	Mean Value of Dust Effect
1	Schedule is defined in contract	Absolute minimum dust effect	Eq. (11)	Contractor is not allowed to select the demolition period for any sub-site	0.4
2	Schedule is defined in contract	Optimal minimum dust effect	Eq. (12)	Contractor is not allowed to select the demolition period for any sub-site	0.44
3	Schedule is defined in contract	Optimal minimum dust effect	Eq. (13)	Contractor is not allowed to select the demolition period for any sub-site	0.42
4	Scheduling is not defined in contract	No constraint	N/A	Contractor has freedom of selection of demolition periods for sub-sites	0.48
5	Schedule is defined in contract	Fictious (N/A)	Fictious (N/A)	Contractor is not allowed to select the demolition period for any sub-site	0.59

11. Conclusions

While it's crucial to choose the appropriate contractor for demolition projects (Dowdell, 2016), government regulations should clearly define the guidelines. Currently, contractors are not required to adhere to a specific schedule outlined by government regulations. This omission can lead to unforeseen circumstances (Chu, 2008), such as contract cancellations and environmental damage. Therefore, it's imperative to establish a methodology for defining demolition schedules that result in cleaner and less hazardous demolitions.

In the present study, a pioneering demolition scheduling methodology is introduced to reduce the impact of dust on humans and the environment. The methodology integrates a dust dispersion model and AHP. The dust dispersion model delineates the region under dust exposure and quantifies the dust concentration in that defined area, while vulnerability rates are determined through AHP analysis. By multiplying exposure rates with vulnerability rates, dust effect rates are computed for the entire site. However, given the variable nature of wind characteristics throughout the year and the differing vulnerabilities of buildings, the demolition region is subdivided into subsites, and the year is segmented into demolition time periods. This process involves determining dust effect rates for each subsite and time period, resulting in a matrix that guides the scheduling of the demolition activity.

To demonstrate the applicability of this methodology, Kahramanmaraş, a city in Türkiye with over 10,000 buildings scheduled for demolition due to a recent destructive earthquake, is used as a case study. Nine subsites in the city center were selected, assuming an equal time for the demolition of each subsite (one month). The analysis is performed for each subsite and each month, resulting in a matrix of dust effect rates (Table 2). Five different schedules are devised using this matrix. The first schedule aims for the absolute minimum dust effect rate by planning the demolition of each subsite during its minimum dust effect month throughout the year. The second schedule achieves optimal minimum dust effect rates by imposing a constraint that only one subsite could be demolished per month. The third schedule is composed to focus on the importance of the objective function used for scheduling. In the fourth schedule, the assumption is made that the contractor has no obligation to follow a specific schedule, allowing for a plan focused on minimizing expenses for the contractor's convenience. The fifth schedule is designed as a worst-case scenario for comparative analysis, although it lacks practicality.

It is essential to note that the defined schedules are unique to the selected site, and variations may occur for the same site by altering the

number of sub-sites and the designated time period. Based on the analysis and defined assumptions, it is observed that, although the third schedule is 5% worse than the first schedule (which defines the absolute minimum dust effect), it mitigates the dust effect by 13% compared to the fourth schedule. In comparison to the worst-case scenario, the first three scenarios achieve a 32%, 29%, and 25% reduction in dust effect, respectively. Even though the worst scenario is not realistic, the substantial difference highlights the efficiency of the proposed methodology.

CRediT authorship contribution statement

Ali Ersin Dinçer: Writing – review & editing, Writing – original draft, Visualization, Validation, Supervision, Software, Resources, Project administration, Methodology, Investigation, Funding acquisition, Formal analysis, Data curation, Conceptualization. **Abdullah Demir:** Writing – review & editing, Writing – original draft, Visualization, Validation, Supervision, Software, Resources, Project administration, Methodology, Investigation, Funding acquisition, Formal analysis, Data curation, Conceptualization. **Ömer Dilmen:** Visualization.

Declaration of competing interest

The authors declare that they have no known competing financial interests or personal relationships that could have appeared to influence the work reported in this paper.

Data availability

Data will be made available on request.

References

Akboğa Kale, Ö., Gürcanlı, G.E., Baradan, S., 2017. Asbestos exposure and prevention methods in urban renewal process. Pamukkale University Journal of Engineering Sciences 23, 694–706. https://doi.org/10.5505/pajes.2016.66049.

Alipour-Bashary, M., Ravanshadnia, M., Abbasianjahromi, H., Asnaashari, E., 2021. A hybrid fuzzy risk assessment framework for determining building demolition safety index. KSCE J. Civ. Eng. 25, 1144–1162.

Bagtzoglou, A.C., Tompson, A.F.B., Dougherty, D.E., 1992. Projection functions for particle-grid methods. Numer. Methods Part. Differ. Equ. 8, 325–340.

Brown, R., 1827. A brief account of microscopical observations made in the months of June. Philos. Mag. A 1–16.

Chu, C., 2008. The myths and politics of housing in Hong Kong: the controversy over the demolition of the Hunghom Estate. Habitat Int. 32, 375–383. https://doi.org/10.1016/j.habitatint.2007.11.002.

Chu, K.H., Lee, K.H., Kim, H.J., Ham, S.H., Ko, K.B., 2011. Comparison and analysis of the dust, water, and soil pollution in explosive demolition sites. Sci. Technol. Energetic Mater. 72, 36–43.

Clark, C., Jambeck, J., Townsend, T., 2006. A review of construction and demolition debris regulations in the United States. Crit. Rev. Environ. Sci. Technol. 36, 141–186. https://doi.org/10.1080/10643380500531197.

Demir, A., 2020. Hydro-elastic analysis of standing submerged structures under seismic excitations with sph-fem approach. Lat. Am. J. Solid. Struct. 17, 1–14. https://doi.org/10.1590/1679-78256266.

Demir, A., Dinçer, A.E., 2023. Efficient disaster waste management: identifying suitable temporary sites using an emission-aware approach after the Kahramanmaraş earthquakes. Int. J. Environ. Sci. Technol. 1–16.

Demir, A., Dinçer, A.E., Çiftçi, C., Gülçimen, S., Uzal, N., Yılmaz, K., 2024. Wind farm site selection using GIS-based multicriteria analysis with life cycle assessment integration. Earth Sci. Inform. 17, 1591–1608.

Demir, A., Dinçer, A.E., Öztürk, Ş., Kazaz, I., 2021. Numerical and experimental investigation of sloshing in a water tank with a fully coupled fluid-structure interaction method, Progress in Computational Fluid Dynamics. Int. J. 21, 103–114.

Demir, A., Dinçer, A.E., Yılmaz, K., 2023. A novel method for the site selection of large-scale PV farms by using AHP and GIS: a case study in İzmir, Türkiye. Sol. Energy 259, 235–245.

Demir, A., Dinçer, A.E., Yılmaz, K., 2024. A novel procedure for the AHP method for the site selection of solar PV farms. Int. J. Energy Res., 5535398

Dinçer, A.E., 2020. Experimental and numerical investigation of hyper-elastic submerged structures strengthened with cable under seismic excitations. European Journal of Environmental and Civil Engineering 1–20. https://doi.org/10.1080/19648189.2020.1837253.

Dinçer, A.E., Demir, A., Yılmaz, K., 2023. Enhancing wind turbine site selection through a novel wake penalty criterion. Energy, 129096.

Dinçer, A.E., Demir, A., Yılmaz, K., 2024. Multi-objective turbine allocation on a wind farm site. Appl. Energy 355, 122346. https://doi.org/10.1016/j.apenergy.2023.122346.

Dinçer, A.E., Dincer, N.N., Tekin-Koru, A, Yaşar, B., Yılmaz, A., 2024. The impact of Kahramanmaraş (2023) earthquakes: A comparative case study for Adıyaman and Malatya. Int. J. Disaster Risk Reduc. 110, 104647. https://doi.org/10.1016/j.ijdrr.2024.104647.

Dorevitch, S., Demirtas, H., Perksy, V.W., Erdal, S., Conroy, L., Schoonover, T., Scheff, P. A., 2006. Demolition of high-rise public housing increases particulate matter air pollution in communities of high-risk asthmatics. J. Air Waste Manage. Assoc. 56, 1022–1032. https://doi.org/10.1080/10473289.2006.10464504.

Dowdell, C., 2016. Importance of selecting a quality demolition contractor. Nat. Gas Electr. 32, 11–14.

Einstein, A., 1905. Über die von der molekularkinetischen Theorie der Wärme geforderte Bewegung von in ruhenden Flüssigkeiten suspendierten Teilchen. Ann. Phys. 4.

Farfel, M.R., Orlova, A.O., Lees, P.S.J., Rohde, C., Ashley, P.J., Chisolm, J.J., 2003. A study of urban housing demolitions as sources of lead in ambient dust: demolition practices and exterior dust fall. Environ. Health Perspect. 111, 1228–1234. https://doi.org/10.1289/ehp.5861.

Heal, M.R., Kumar, P., Harrison, R.M., 2012. Particles, air quality, policy and health. Chem. Soc. Rev. 41, 6606–6630.

Holmes, N.S., Morawska, L., 2006. A review of dispersion modelling and its application to the dispersion of particles: an overview of different dispersion models available. Atmos. Environ. 40, 5902–5928.

Jacobs, D.E., Cali, S., Welch, A., Catalin, B., Dixon, S.L., Evens, A., Mucha, A.P., Vahl, N., Erdal, S., Bartlett, J., 2013. Lead and other heavy metals in dust fall from single-family housing demolition. Publ. Health Rep. 128, 454–462.

Kuo, J.Y.J., Romero, D.A., Beck, J.C., Amon, C.H., 2016. Wind farm layout optimization on complex terrains – integrating a CFD wake model with mixed-integer programming. Appl. Energy 178, 404–414. https://doi.org/10.1016/j.apenergy.2016.06.085.

Liu, C., Pun, S., 2004. Information System Strategy for Promoting Demolition Project Management.

Martin, J.L., McCutcheon, S.C., 1998. Hydrodynamics and Transport for Water Quality Modeling, vol. 816.

McCutcheon, S.C., 1990. Water Quality Modeling: River Transport and Surface Exchange. CRC press.

Menon, N., George, G., Ranith, R., Sajin, V., Murali, S., Abdulaziz, A., Brewin, R.J.W., Sathyendranath, S., 2021. Citizen science tools reveal changes in estuarine water quality following demolition of buildings. Rem. Sens. 13. https://doi.org/10.3390/rs13091683.

Moeller, J.C., Adams, E.E., 1993. Comparison of Eulerian-Lagrangian, random walk and hybrid methods of modeling pollutant transport. In: Estuarine and Coastal Modeling. ASCE, pp. 609–623.

Mølgaard, E.F., Hannerz, H., Tüchsen, F., Brauer, C., Kirkeskov, L., 2013. Chronic lower respiratory diseases among demolition and cement workers: a population-based register study. BMJ Open 3. https://doi.org/10.1136/bmjopen-2012-001938.

Mucha, A.P., Stites, N., Evens, A., MacRoy, P.M., Persky, V.W., Jacobs, D.E., 2009. Lead dustfall from demolition of scattered site family housing: developing a sampling methodology. Environ. Res. 109, 143–148. https://doi.org/10.1016/j.envres.2008.10.010.

Normohammadi, M., Kakooei, H., Omidi, L., Yari, S., Alimi, R., 2016. Risk assessment of exposure to silica dust in building demolition sites. Saf Health Work 7, 251–255. https://doi.org/10.1016/j.shaw.2015.12.006.

Patel, D.J., Patel, D.A., 2020. Assessing the potential health hazards of workers of demolition sector. In: Construction Research Congress 2020: Safety, Workforce, and Education, pp. 414–423. https://doi.org/10.1061/9780784482872.045.

Patel, J., Savsani, V., Patel, V., Patel, R., 2017. Layout optimization of a wind farm to maximize the power output using enhanced teaching learning based optimization technique. J. Clean. Prod. 158, 81–94. https://doi.org/10.1016/j.jclepro.2017.04.132.

Periáñez, R., Elliott, A.J., 2002. A particle-tracking method for simulating the dispersion of non-conservative radionuclides in coastal waters. J. Environ. Radioact. 58, 13–33.

Perkins, R.A., Hargesheimer, J., Fourie, W., 2007. Asbestos release from whole-building demolition of buildings with asbestos-containing material. J. Occup. Environ. Hyg. 4, 889–894. https://doi.org/10.1080/15459620701691023.

Rabito, F.A., Iqbal, S., Shorter, C.F., Osman, P., Philips, P.E., Langlois, E., White, L.E., 2007. The association between demolition activity and children's blood lead levels. Environ. Res. 103, 345–351. https://doi.org/10.1016/j.envres.2006.09.011.

Rahmat, Z.G., Niri, M.V., Alavi, N., Goudarzi, G., Babaei, A.A., Baboli, Z., Hosseinzadeh, M., 2017. Landfill site selection using GIS and AHP: a case study: behbahan, Iran. KSCE J. Civ. Eng. 21, 111–118. https://doi.org/10.1007/s12205-016-0296-9.

Rekik, S., El Alimi, S., 2023. Optimal wind-solar site selection using a GIS-AHP based approach: a case of Tunisia. Energy Convers. Manag. X 18. https://doi.org/10.1016/j.ecmx.2023.100355.

Rodríguez, R., Garcia-Gonzalez, H., Pastrana, Á., Hernández, Z., 2023. Health and safety protocol for the management of building demolition waste with high mercury contamination. Buildings 13. https://doi.org/10.3390/buildings13051310.

Salamon, P., Fernàndez-Garcia, D., Gómez-Hernández, J.J., 2006. A review and numerical assessment of the random walk particle tracking method. J. Contam. Hydrol. 87, 277–305.

Sutherlan, W., 1904. The measurement of large molecular masses. In: Proceedings of the 10th Meeting of the Australasian Association for the Advancement of Science, Dunedin, pp. 117–121.

Sutherland, W., 1905. LXXV. A dynamical theory of diffusion for non-electrolytes and the molecular mass of albumin. London, Edinburgh Dublin Phil. Mag. J. Sci. 9, 781–785.
Velioglu, D., Denli Tokyay, N., Ersin Dincer, A., 2015. A numerical and experimental study on the characteristics of hydraulic jumps on rough beds. In: 36th IAHR World Congress, Hague.
Venkatram, A., Isakov, V., Pankratz, D., Heumann, J., Yuan, J., 2004. The analysis of data from an urban dispersion experiment. Atmos. Environ. 38, 3647–3659.
Yılmaz, K., Dinçer, A.E., Ayhan, E.N., 2023. Exploring flood and erosion risk indices for optimal solar PV site selection and assessing the influence of topographic resolution. Renew. Energy, 119056.
Yu, T., Shen, G.Q., Shi, Q., Zheng, H.W., Wang, G., Xu, K., 2017. Evaluating social sustainability of urban housing demolition in Shanghai, China. J. Clean. Prod. 153, 26–40. https://doi.org/10.1016/j.jclepro.2017.03.005.
Zhao, L., Chen, Z., Lee, K., 2011. Modelling the dispersion of wastewater discharges from offshore outfalls: a review. Environ. Rev. 19, 107–120.

GCRIS